

## VESTIGE OF THE STAR CLUSTER BURST IN M51<sup>\*</sup>

NARAE HWANG<sup>1,2,3</sup> AND MYUNG GYOON LEE<sup>2</sup>

<sup>1</sup> National Astronomical Observatory of Japan  
2-21-1 Osawa Mitaka, Tokyo 181-8588, Japan and

<sup>2</sup> Astronomy Program, Department of Physics and Astronomy,  
Seoul National University, Seoul 151-747, Korea

*Accepted for publication in Astrophysical Journal*

### ABSTRACT

We present a study of the star cluster formation in M51 based on the image data taken with Advanced Camera for Surveys (ACS) and Wide Field Planetary Camera 2 (WFPC2) of Hubble Space Telescope (HST). We have derived the star cluster formation rate using the ages and masses of about 2,000 star clusters estimated by comparing photometric data ( $F336W$ ,  $F435W$ ,  $F555W$ , and  $F814W$ ) with theoretical population synthesis models. The star cluster formation rate increased significantly during the period of 100 ~ 250 Myr ago. This period roughly coincides with the epoch of dynamical encounters of two galaxies, NGC 5194 and NGC 5195, expected by theoretical models. The age distribution of the star clusters also shows two peaks at about 100 Myr and 250 Myr ago. The star cluster mass ranges from  $10^3$  to  $10^6 M_{\odot}$  and the mass function can be represented by a power law with an index ranging from  $\alpha = -2.23 \pm 0.34$  for  $t < 10$  Myr to  $\alpha = -1.37 \pm 0.11$  for  $t > 100$  Myr. The mass function of star clusters older than 10 Myr also appears to display the steepest distribution with  $\alpha \approx -1.50$  at around 200 Myr ago, near the expected epoch of the galaxy interaction. We also confirm the correlations of cluster size increasing with cluster mass (with a best fit slope of  $0.16 \pm 0.02$ ), and with cluster age ( $0.14 \pm 0.03$ ).

*Subject headings:* galaxies: individual (M51; NGC 5194; NGC 5195) — galaxies: interaction — galaxies: spiral — galaxies: starburst — galaxies: star clusters

### 1. INTRODUCTION

Star clusters are an excellent tool to probe the formation and evolution of galaxies due to their high brightness enough to be detected even in some nearby galaxies. They are considered to be composed of stars that formed at the same time. Some star clusters are also known for their longevity: globular clusters are as old as the Universe itself. Therefore, we can investigate the very ancient star cluster formation events as well as the recent ones in a galaxy by estimating the age of star clusters and constructing their age distribution.

M51 is an interacting galaxy system that is composed of a Sbc galaxy (NGC 5194) and a fainter SB0 galaxy (NGC 5195). M51 is an optimal and interesting target for the study of star cluster formation for several reasons. (1) It is abundant with interstellar media (see a recent study by Schuster et al. 2007 and references therein) that serve as basic ingredients for stars and star clusters. HII region studies (e.g., Scoville et al. 2001, Lee, J. H. 2009 in preparation) showed that current formation of stars and star clusters is actively going on in M51. (2) There are some theoretical (Toomre & Toomre 1972; Salo & Laurikainen 2000) and observational (Durrell et al. 2003) studies suggesting that the two galaxies in M51 experienced a single or multiple encounters some hundred Myr ago. Therefore it is possible to find any correlations between these dy-

namical events and the star formation events in M51. (3) M51 is located at a distance of 8.4 Mpc (Feldmeier et al. 1997) so that, with the resolving power of the Hubble Space Telescope (*HST*), it is possible to resolve, at least, some star clusters in M51.

Several studies used the *HST* data to survey star clusters in M51. Bik et al. (2003) detected about 1000 star clusters in a small region near the center of M51 and found that the cluster formation rate decreases with age during the period of 10 – 1000 Myr ago. However, they found no evidence for an increased cluster formation rate around 200 – 400 Myr ago, when the first encounter of NGC 5194 and NGC 5195 was expected. Bastian et al. (2005) showed that the cluster formation rate increased about 50 – 70 Myr ago when the second (or last) passage of NGC 5195 was expected by a multiple passage model (Salo & Laurikainen 2000). Still, no clear sign of increased star cluster formation around the 200 – 400 Myr ago was shown by Bastian et al. (2005). A hint on the increased cluster formation rate around this epoch was given by Lee et al. (2005). They derived the age distribution of about 400 resolved clusters in M51 using the *HST* archival data and showed that, when compared with another typical late type galaxy M101, there are an increased number of star clusters with ages of 100 – 500 Myr, which are consistent with the expected epoch of the first encounter. However, their study did not cover the entire area of M51 and the number of star clusters used in their study was small.

One limiting factor that has haunted previous studies on star clusters in M51 is the limited field of view and the insufficient depth of the available data. It became possible to reduce this problem, when the deep and

<sup>\*</sup> Based on observations made with the NASA/ESA *Hubble Space Telescope*, obtained from the data archive at the Space Telescope Science Institute, which is operated by the Association of Universities for Research in Astronomy, Inc., under NASA contract NAS 5-26555.

<sup>3</sup> Japan Society of the Promotion of Science Research Fellow

wide field image data taken with the Advanced Camera for Surveys (ACS) onboard the *HST* were released (Mutchler et al. 2005). Now it enables to investigate the star clusters concentrated not only in the disk of NGC 5194 but also those around the outer halo including the companion galaxy NGC 5195 in a homogeneous quality. This has led to several new studies on the star clusters in M51: Hwang & Lee (2006) on faint fuzzy clusters in NGC 5195, Scheepmaker et al. (2007) on the cluster size distribution, Hwang & Lee (2008) on the photometric properties of star clusters, Haas et al. (2008) on the cluster luminosity function, and Scheepmaker et al. (2009) on the distribution of star cluster formation in the disk. However, there is not yet any detailed study using this new data on the correlation between the star cluster formation and dynamical interactions in M51, and it is not yet clear how the star cluster formation was affected by the dynamical events in M51.

In this study, we investigate the age distribution of M51 star clusters and derive the cluster formation rate using the catalog of the star clusters in M51 given by Hwang & Lee (2008). This star cluster catalog includes about 3,600 clusters with  $V_{F555W} < 23$  mag and provides photometric data in  $F435W$ ,  $F555W$ , and  $F814W$  bands. We compare the photometric data in this catalog with the population synthesis models by Bruzual & Charlot (2003) to estimate the age and mass of star clusters. A preliminary study of the age distribution of M51 star clusters was already presented in Hwang & Lee (2007), implying a possible correlation between the dynamical encounters of galaxies and the age distribution of star clusters in M51. However, this result was based on  $F435W$ ,  $F555W$ , and  $F814W$  band photometry data, and could be severely affected by the age-reddening degeneracy in age estimation. Therefore, we included the  $F336W$  band image data of M51 taken with *HST* WFPC2 to improve the accuracy of age estimation for this study.

The organization of this paper is as follows: Section 2 describes the data. Section 3 briefly introduces the star cluster selection and photometry procedures along with the reduction of  $F336W$  band data. Section 4 describes the age estimation method. We present the main results including the age and mass distribution, and the star cluster formation rate in Section 5. We discuss the primary results in Section 6. Finally, a summary and conclusion is given in Section 7.

## 2. DATA

The main data used in this study are  $F435W$ ,  $F555W$ , and  $F814W$  band images taken with *HST* ACS through the Hubble Heritage program 10452 (PI: S. V. W. Beckwith). We also used the  $F336W$  band images taken with *HST* WFPC2 for six fields through the observing program 10501 (PI: R. Chandar), and another  $F336W$  band image set that covered the central region of NGC 5194, available in the *HST* archive. A brief information on the  $F336W$  band data set is provided in Table 1. Figure 1 shows the observed fields overlaid on the  $12' \times 12'$  Digitized Sky Survey (DSS) image of M51. Seven WFPC2  $F336W$  fields cover a major part of M51, but their coverage is still much smaller than the ACS field.

Data reductions for ACS data were carried out by the STScI including multi-drizzling and image combi-

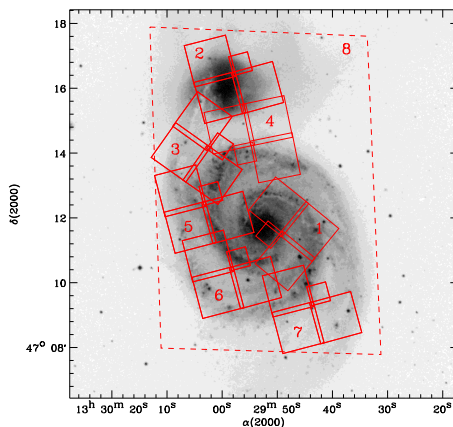


FIG. 1.— Locations of the fields with the *HST* ACS data (field #8 in dashed line) and WFPC2 data (solid line) used in this study overlaid on a  $12' \times 12'$  Digitized Sky Survey image of M51. Detailed information on each pointing is listed in Table 1.

nation. More detailed information on these *HST* ACS data reductions was given in Mutchler et al. (2005).<sup>3</sup> All WFPC2 data that were retrieved from the *HST* archive were reduced using the “on-the-fly” calibration, which automatically uses the best reference files for calibration. The WFPC2 data reduction steps include bad pixel masking, analog-to-digital correction, bias and dark subtraction, and flat-field correction. There are two individual images per each WFPC2 pointing. These two WFPC2 image data were combined using the *combine* task in STSDAS package of IRAF<sup>4</sup> with CRREJECT option in order to eliminate cosmic rays and increase the signal-to-noise ratio.

We adopted a distance of  $8.4 \pm 0.6$  Mpc [ $(m - M)_0 = 29.62$ ] to M51 determined from the planetary nebula luminosity function in M51 (Feldmeier et al. 1997). The corresponding linear scale is  $40.7$  pc arcsec<sup>-1</sup>. The foreground reddening toward M51 is low,  $E(B - V) = 0.035$ , and the corresponding extinctions are  $A_B = 0.150$ ,  $A_V = 0.115$ ,  $A_I = 0.067$ , and  $A_U = 0.190$  mag (Schlegel et al. 1998). The total magnitudes and colors are  $B^T = 8.96 \pm 0.06$  mag and  $(B^T - V^T) = 0.60 \pm 0.01$  for NGC 5194, and  $B^T = 10.45 \pm 0.07$  mag and  $(B^T - V^T) = 0.90 \pm 0.01$  for NGC 5195 (de Vaucouleurs et al. 1991). At the adopted distance (without internal extinction correction), the absolute magnitudes are  $M_B^T = -20.81$  mag,  $M_V^T = -21.38$  mag for NGC 5194, and  $M_B^T = -19.32$  mag and  $M_V^T = -20.19$  mag for NGC 5195.

## 3. STAR CLUSTER SELECTION AND PHOTOMETRY

We detected and classified star clusters in M51 based on *HST* ACS data and made a catalog of the star clusters with  $F555W < 23$  mag. Detailed information on star cluster detection, photometry, and classification was

<sup>3</sup> See also <http://archive.stsci.edu/prepds/m51/>.

<sup>4</sup> IRAF is distributed by the National Optical Astronomy Observatory, which is operated by the Association of Universities for Research in Astronomy (AURA) under cooperative agreement with the National Science Foundation.

TABLE 1  
A LIST OF *HST* WFPC2 *F336W* BAND DATA FOR M51 USED IN THIS STUDY

Field No.	Prop. ID	RA (J2000) [hh mm ss]	Dec (J2000) [dd mm ss]	Instruments	Filters	Exposure Times [sec]
1	7375	13 29 47.81	+47 11 32.84	WFPC2	<i>F336W</i>	2 x 600
2	10501	13 30 00.52	+47 15 40.40		<i>F336W</i>	2 x 1300
3		13 30 07.80	+47 14 00.50		<i>F336W</i>	2 x 1300
4		13 29 51.68	+47 15 02.85		<i>F336W</i>	2 x 1300
5		13 30 05.90	+47 11 40.00		<i>F336W</i>	2 x 1300
6		13 30 00.87	+47 09 39.37		<i>F336W</i>	2 x 1300
7		13 29 46.32	+47 08 34.39		<i>F336W</i>	2 x 1300

described in Hwang & Lee (2008) and only a brief summary is provided here.

We carried out the source detection in the background-subtracted *F555W* band image of ACS data using SExtractor (Bertin & Arnouts 1996). A detection threshold of  $4\sigma$  and minimum contiguous detected area of 5 pixels were used for finding sources. The flux of the detected objects was measured using SExtractor in dual mode for the *F435W*, *F555W*, and *F814W* band images. An aperture with  $r = 6$  pixels ( $0.3'' \simeq 12$  pc) was adopted for the photometry. The instrumental magnitudes in the *F435W*, *F555W*, and *F814W* bands were calibrated using the photometric zero points of the Vega magnitude system for the *HST* ACS/WFC provided by Sirianni et al. (2005). We visually inspected candidate sources with *F555W* < 23 mag considering their radial profile, morphology, and environmental conditions. We selected and classified star clusters into two different categories: Class 1 star clusters that have a circular shape and no prominent nearby neighbors; and Class 2 star clusters that have an elongated shape and/or irregular structure, and/or multiple neighbors. Finally, we selected 2,224 Class 1 and 1,388 Class 2 star clusters with *F555W* < 23 mag and their catalog was provided in Hwang & Lee (2008).

We carried out an independent source detection and photometry in the *F336W* WFPC2 image data. Sources in WFPC2 image data were detected using SExtractor with a detection threshold of  $3\sigma$  and minimum contiguous detected area of 3 pixels ( $0''.3$ ). The flux of detected sources was measured using an aperture with  $r = 0''.3$  (6 pixels for PC and 3 pixels for WF) in SExtractor. The instrumental magnitudes in *F336W* were calibrated using the photometric zero points of the Vega magnitude system for WFPC2 listed in the *HST* Data Handbook for WFPC2. A correction for the charge transfer efficiency (CTE) loss was made based on the prescription given by Dolphin (2000).<sup>5</sup> The coordinates of the detected sources were derived using *metric* task in STSDAS package of IRAF that corrects for the geometric distortion of each chip in WFPC2. The derived coordinates of sources in WFPC2 data were calibrated to the system of *HST* ACS data.

We compared the *F336W* band catalog with the catalog derived from the *F435W*, *F555W*, and *F814W* band data. There are about 1,400 Class 1 and about 1,000 Class 2 star clusters that have counterparts detected in the *F336W* band within a matching radius of  $0''.4$ .

<sup>5</sup> See [http://purcell.as.arizona.edu/wfpc2\\_calib/](http://purcell.as.arizona.edu/wfpc2_calib/) for further updated information.

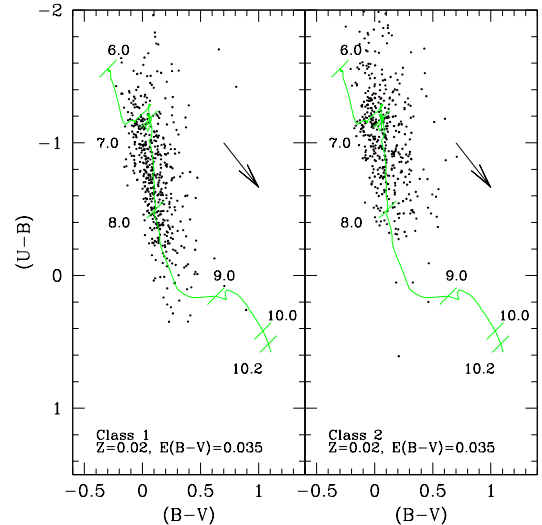


FIG. 2.—  $(B - V) - (U - B)$  diagrams of the Class 1 star clusters (left panel) and Class 2 star clusters (right panel) with  $V < 23$  mag in M51. The solid line represents a theoretical evolutionary track with  $Z = 0.02$  by Bruzual & Charlot (2003) shifted according to the foreground reddening  $E(B - V) = 0.035$ . Numbers that run from 6.0 to 10.2 with tick marks on the track represent  $\log(\text{age})$ . The arrow in each panel shows the direction of reddening corresponding to  $E(B - V) = 0.3$ .

We checked the spatial distribution of the sources that have no *F336W* band counterpart and the locations of WFPC2 observation fields to separate star clusters that do not emit a significant flux in the *F336W* band from those that were not covered in the *F336W* band observations. It is found that the number of star clusters that were not observed in the *F336W* band is about 300 for Class 1 and about 80 for Class 2. Hereafter, we use  $U$ ,  $B$ ,  $V$ , and  $I$  to denote *F336W*, *F435W*, *F555W*, and *F814W*, respectively.

Figure 2 shows the  $(B - V) - (U - B)$  color-color diagram for the star clusters (Class 1 and Class 2) in M51. We also display a theoretical evolutionary track for the simple stellar population of Bruzual & Charlot (2003) with metallicity  $Z = 0.02$ , shifted according to the foreground reddening  $E(B - V) = 0.035$ . It is seen that most star clusters detected in  $U$  band are blue with  $(U - B) < 0.2$  and younger than 1 Gyr. There are only a few Class 2 star clusters with  $(U - B) > -0.4$  (older than about 100 Myr in age), while there are still many Class 1 star clusters with  $-0.4 < (U - B) < 0.0$ . It is noted that the  $(U - B)$  color for the blue clusters varies from  $-1.8$  to  $-0.2$ , while the  $(B - V)$  color varies only from  $0.2$  to  $-0.2$ . This shows the usefulness of  $U$  band

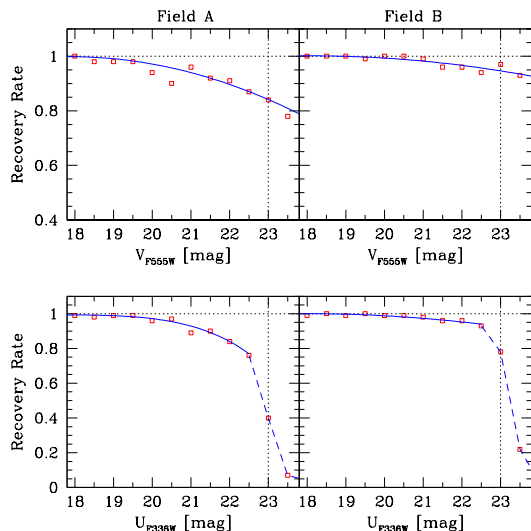


FIG. 3.— Recovery rates of artificial star clusters as a function of magnitudes in  $V$  and  $U$  band derived from Field A (with higher crowding) and B (with lower crowding). Solid lines are polynomial fits to the data and dashed lines are straight lines connecting data points.

photometry in estimating the age of young star clusters.

We tested the completeness of star cluster detection in  $V$  and  $U$  band images. Since the efficiency of star cluster detection can be affected by the degree of source crowding, we selected two separate fields with different source crowding for this test: Field A ( $\alpha = 13 : 30 : 03.2$ ,  $\delta = +47 : 13 : 32.6$ ) with higher crowding and Field B ( $\alpha = 13 : 30 : 05.8$ ,  $\delta = +47 : 11 : 49.5$ ) with lower crowding. Each field was set to a square with size of about  $1' \times 1'$ . The selected two fields were covered in both  $V$  and  $U$  bands. Artificial star clusters were generated using *mkobjects* task of ARTDATA package in IRAF. The point spread function (PSF) images required for artificial cluster generation were prepared in ACS  $V$  band data and in WFPC2  $U$  band data.

We generated 120 artificial clusters in one test field image over the magnitude range of  $18 \sim 23.5$  mag with 0.5 mag step (10 artificial clusters per each magnitude step). The FWHM and ellipticity of artificial clusters were derived from the observed size and ellipticity distribution of M51 star clusters in Table 1 of Hwang & Lee (2008). To do that, we modeled observed distributions using a Gaussian centered at 3.25 pixels with  $\sigma = 2.0$  for FWHM and another Gaussian centered at 0.15 with  $\sigma = 0.25$  for ellipticity. Then, FWHM and ellipticity were randomly derived from these Gaussian distributions and assigned to each artificial cluster. However, we selected only artificial clusters with FWHM  $> 2.0$  pixels to be consistent with the observed data. We randomly distributed artificial clusters in a test field image and carried out source detection and photometry in the same way as it was done for M51 star clusters. This routine of test was repeated 10 times in each test field and the results of source detection and photometry were compared with the input model parameters to calculate the completeness of our star cluster photometry data.

Figure 3 shows the result of the completeness test for Field A (high crowding) and Field B (low crowding). It can be seen that the recovery rate (completeness) of ar-

tificial clusters with  $V < 23$  mag is higher than 80% ( $> 84\%$  for Field A and  $> 93\%$  for Field B). However, the recovery rate of artificial clusters with  $U = 23$  mag drops to about 40% in Field A and about 80% in Field B. This shows that the number of star clusters that we may have failed to detect increases more significantly in the  $U$  band than in the  $V$  band as the clusters get fainter. However, it is noted that the recovery rate of star clusters is higher than 80% when star clusters are brighter than  $U = 22$  mag (84% for Field A and 96% for Field B). This value is consistent with the recovery rate of star clusters with  $V = 23$  mag, the magnitude limit adopted for the star cluster survey in Hwang & Lee (2008).

#### 4. AGE AND MASS ESTIMATION

We compared the photometric data of M51 star clusters with the model spectral energy distribution (SED) to estimate the ages and masses of the star clusters. Model SEDs were derived from the theoretical evolutionary synthesis model by Bruzual & Charlot (2003). For these models we adopted a Salpeter initial mass function with a power slope of  $x = -2.35$  (Salpeter 1955), a lower mass cutoff of  $0.1 M_{\odot}$  and an upper mass cutoff of  $100 M_{\odot}$ . The models span ages from 1 Myr to 15 Gyr for metallicity range of  $Z = 0.0001 \sim 0.05$ . However, due to the age-metallicity-reddening degeneracy in the integrated colors of star clusters, we assume the solar metallicity for our working models to derive only age and reddening. Observations of the HII regions in M51 shows that the current metallicity of the gas in this galaxy is approximately solar (e.g., Diaz et al. 1991; Hill et al. 1997). It is also known that the influence of metallicity becomes more pronounced for old star clusters with age of  $> 1$  Gyr in their integrated colors. Because the majority of star clusters in M51 is expected to be younger than 1 Gyr from the study in Bastian et al. (2005) and Hwang & Lee (2008), the adoption of the solar metallicity is considered appropriate.

We compared an SED model with a certain age to the observed data for each star cluster, after reddening the model by  $E(B - V)$  values between 0.0 and 0.6 in steps of 0.015, for about 2,400 star clusters with  $UBVI$  photometry. This range includes the reddening values derived from the previous studies for the most star clusters in M51. Lamers et al. (2002) showed that the reddening in the bulge of NGC 5194 is typically  $E(B - V) \approx 0.2$  and Lee et al. (2005) also reported that most star clusters in M51 appear to have associated reddening  $E(B - V) < 0.1$ . For every combination of age and  $E(B - V)$ , we fitted the theoretical SED models to the observed photometric data and calculated the  $\chi^2$ . The fit with a minimum  $\chi^2$  was adopted as the best fit for the age and  $E(B - V)$  combination.

The number of finally accepted fits is 1,125 for Class 1 and 835 for Class 2 star clusters. Then we derived the masses for these star clusters by combining the  $M/L_V$  ratio of the best fit model with the measured  $V$  band cluster luminosity, extinction, and the distance to M51. Figure 4 shows the age versus mass diagram for these star clusters. The solid curve indicates the magnitude limit of  $V = 23$  mag adopted for star cluster selection in Hwang & Lee (2008). The other lines show the expected age and mass of star clusters with different  $U$  band magnitude ranging from 23 to 21.5 mag. This shows that

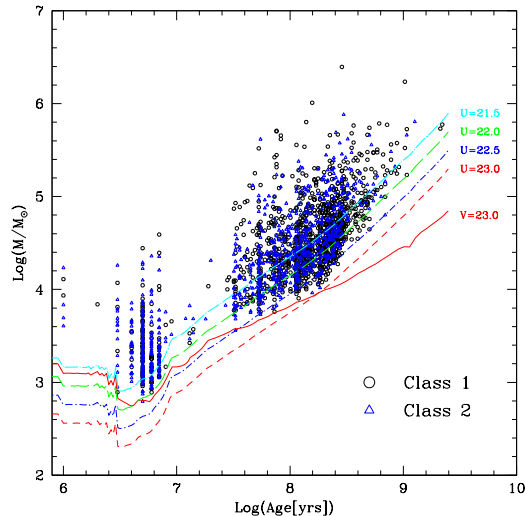


FIG. 4.— Mass vs. age of the star clusters in M51 (circles for Class 1 and triangles for Class 2). The solid line shows the magnitude limit of  $V = 23$  mag used to select star clusters in Hwang & Lee (2008). Other lines display magnitude limits in the  $U$  band.

star clusters with 1 Gyr are detected only if they are more massive than  $10^{5.2} M_{\odot}$  (brighter than  $U \approx 22$  mag) as indicated in Figure 4. Note that the completeness for  $U = 22$  mag band is 80% as shown in Figure 3.

Several features are noted in Figure 4. First, there is a region with few star clusters between  $\log t = 7$  and  $7.5$  ( $t$  represents an age in units of years). This is considered to be an artifact that is caused by the age-dating techniques that compare the integrated colors of star clusters with the synthesis models. In this age range, the predicted colors of star clusters span a very narrow range of colors, e.g.,  $\delta(U - B) \approx 0.16$  mag,  $\delta(B - V) \approx 0.00$  mag, and  $\delta(V - I) \approx 0.22$  mag in the models by Bruzual & Charlot (2003). Therefore, even a small photometric error can result in a fit to star cluster age younger than  $\log t = 7$  or older than  $\log t = 7.5$ . Second, there are two age regions of over abundance in star clusters: one with  $\log t \leq 7$  and the other with  $7.5 < \log t < 9.0$ . The over-density at  $\log t \leq 7$  is suspected to be, in part, due to the under-density at  $7.0 < \log t < 7.5$ . Nonetheless, it is still a sign that shows the existence of many young star clusters, which is consistent with the results of several studies on HII regions (e.g., Scoville et al. 2001; Lee, J. H. et al. 2009 in preparation). The other over-density at  $7.5 < \log t < 9.0$  indicates that many star clusters were actually formed in this epoch. Third, there is an apparent trend that the mass of the most massive clusters increases with age. This is known as a ‘size-of-sample effect’ noted by Hunter et al. (2003). However, it seems that the upper limit of this relation is composed of multiple components. We discuss this further in Section 6.2.

Similar features in the age and mass distribution were also reported in several other studies of M51 star clusters. For example, the under-density of star clusters in  $7.0 < \log t < 7.5$  can be noted in the results given by Bastian et al. (2005) (their Figure 10) and Gieles et al. (2005) (their Figure 1) in combination with the strong over-density of star clusters with  $\log t < 7$ . This is consistent with the result shown in Figure 4. However, Scheepmaker et al. (2009) show rather different age and

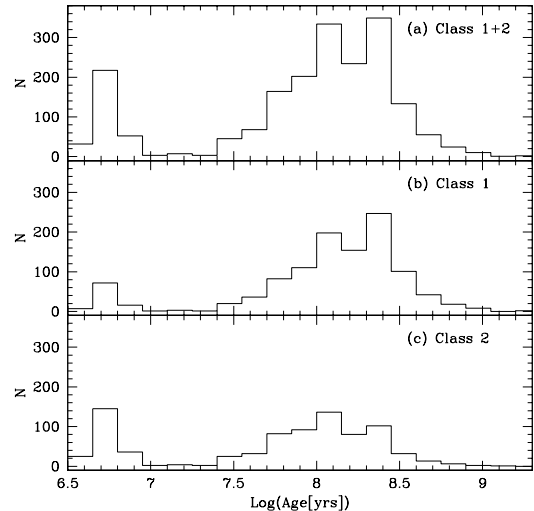


FIG. 5.— Age distributions of the star clusters in M51:(a) all (Class 1 and 2) clusters, (b) Class 1 clusters, and (c) Class 2 clusters. Three peaks at  $\log t \approx 6.7, 8.0,$  and  $8.4$  are noted.

mass distributions in their study of M51 star clusters using the same data that are used in this study. Most star clusters in the sample of Scheepmaker et al. (2009) are found to be younger than  $\log t = 7.5$  and there is no evident feature of under-density in  $7.0 < \log t < 7.5$ , which is contrary to the results of other studies (Bastian et al. 2005; Gieles et al. 2005) as well as this study. One of the possible reasons for this difference may be different criteria adopted for star cluster selection, which may lead to a different sample of star clusters used for the analysis.

Another noteworthy point shown in Scheepmaker et al. (2009) is that different population synthesis models can introduce a systematic change to the derived age and mass distributions of star clusters. However, the result of their study shown in their Figure 4 reveals that the age distribution of star clusters with  $\log t \geq 8$  is found to be more-or-less consistent with one another even in the case that different isochrones (Padova or Geneva) and different metallicities are adopted for models. Considering these inconsistencies and limits caused by the different analysis methods adopted, we focus on the age and mass distributions of star clusters with  $\log t > 7.5$ .

## 5. RESULTS

### 5.1. Star Cluster Age Distribution

Figure 5 shows the age distributions of all star clusters (including both Class 1 and Class 2), Class 1 star clusters, and Class 2 star clusters. It is clear that the age distributions display two over-dense epochs: one with  $\log t < 7$  and another with  $7.5 < \log t < 9.0$ . The over-densities of star clusters in these two periods are evident in the age distribution of both Class 1 and Class 2 star clusters, as shown in Figures 5(b) and (c). However, about 1000 Class 1 star clusters are found in the epoch of  $7.5 < \log t < 9.0$ , while only about 100 Class 1 star clusters are younger than  $\log t = 7$ . On the other hand, for Class 2 star clusters, the number of Class 2 star clusters younger than  $\log t = 7$  is about 230, about one third of the number of star clusters with  $7.5 < \log t < 9.0$ .

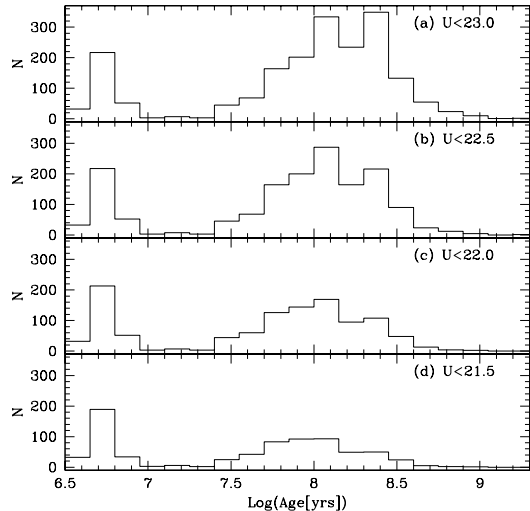


FIG. 6.— Age distributions of the star clusters in M51 for different  $U$  band magnitude limits: (a)  $U < 23.0$  mag, (b)  $U < 22.5$  mag, (c)  $U < 22.0$  mag, and (d)  $U < 21.5$  mag. Note that three peaks at  $\log t \approx 8.0$  and  $8.4$  are visible clearly in all panels, and the oldest peak at  $\log t \approx 8.4$  is weak for the brightest limit  $U < 21.5$  mag.

One interesting point is that there are distinct features in the age range of  $7.5 < \log t < 9.0$  in Figure 5(a). The most pronounced one is a broad component over  $\log t \approx 7.8 - 8.5$  that displays two peaks at  $\log t \approx 8.0$  and  $\log t \approx 8.4$ . The same broad component is also present in the distributions of Class 1 and Class 2 star clusters shown in Figures 5(b) and (c), respectively. However, for Class 1 star clusters, the peak at  $\log t \approx 8.4$  is more enhanced than that at  $\log t \approx 8.0$ . On the other hand, the peak at  $\log t \approx 8.0$  is relatively more significant in case of Class 2 star clusters. Other than these, the age distributions of Class 1 and Class 2 clusters are consistent with each other. Therefore, we consider the age distribution of all star clusters including Class 1 and Class 2 clusters for the further analysis.

We investigated the effect of incompleteness to the age distribution of star clusters. As shown in Figure 4, the incompleteness with different  $U$  band magnitudes may bias the interpretation of age distribution. Therefore, we derived the age distribution of star clusters changing the limiting  $U$  band magnitude starting from  $U = 23.0$  to  $21.5$  mag, and showed the results in Figure 6. Although the amplitude of histograms in  $7.5 < \log t < 9.0$  is gradually decreasing as the  $U$  band magnitude limit gets brighter from  $U < 23$  to  $U < 22$  mag, the overall features in the age distribution remain consistent. Even when the  $U$  band magnitude limit is raised to  $U = 21.5$  mag, where the completeness is estimated to be about 90% (see Figure 3), some hint of peaks at  $\log t \approx 8.0$  and  $\log t \approx 8.4$  can be noticed, as shown in Figure 6(d). This indicates that the two peaks at  $\log t \approx 8.0$  and  $\log t \approx 8.4$  in the age distribution of star clusters shown in Figure 5 are reliable against any incompleteness problem expected from the photometry.

## 5.2. Star Cluster Mass Function

Figure 7 shows the mass functions of all star clusters (including both Class 1 and Class 2), Class 1 star clusters, and Class 2 star clusters in M51. It is found that the

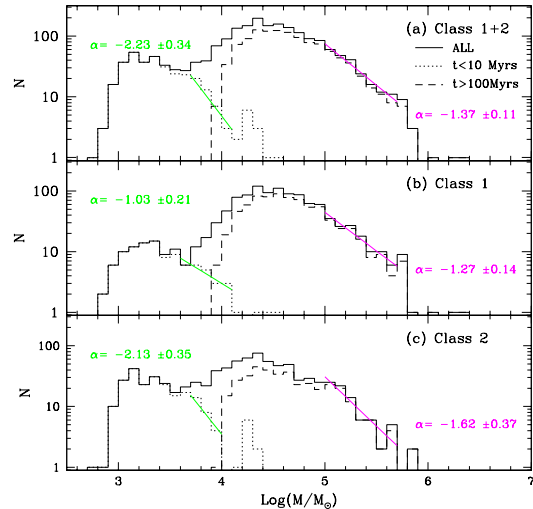


FIG. 7.— Mass functions of the star clusters in M51: (a) all (Class 1 and 2) clusters, (b) Class 1 clusters, and (c) Class 2 clusters (solid line histograms). Dotted line and dashed line histograms represent very young star clusters with  $t < 10$  Myr, and the intermediate-age star clusters with  $t > 100$  Myr, respectively. Solid lines represent power law fits (linear fits in the logarithmic scales) for given mass ranges.

mass of star clusters in M51 ranges from  $10^3$  to  $10^6 M_\odot$  for both Class 1 and Class 2 star clusters and that the overall mass function appears to be separated into two components by a dip at  $\approx 10^{3.7} M_\odot$ . This dip, separating low mass and high mass clusters, is caused by an artifact of the SED fitting method over  $\log t = 7.0 - 7.5$  as described in Section 4 and the star cluster detection limit of  $V < 23$  mag adopted in this study, as shown in Figure 4. The star clusters with different masses also represent star clusters with different ages, as shown in each panel of Figure 7: the low mass star clusters are younger than 10 Myr old (dotted lines) and the high mass star clusters are mostly older than 100 Myr old (dashed lines).

The mass functions of young ( $< 10$  Myr) and intermediate-age/old ( $> 100$  Myr) star clusters can be represented with a power law over the range of  $3.6 < \log(M/M_\odot) < 4.1$  for young clusters and  $5.0 < \log(M/M_\odot) < 5.7$  for intermediate-age/old clusters, regardless of Class 1 or Class 2. It is noted that the upper limit for intermediate-age/old clusters is marked by a weak bump at  $\log(M/M_\odot) \sim 5.8$ , as shown in each panel of Figure 7. We derived a power law index  $\alpha$  of the cluster mass function as defined in  $NdM \propto M^\alpha dM$ . It is found from the sum of Class 1 and Class 2 clusters that the power law index  $\alpha$  for old star clusters with  $5.0 < \log(M/M_\odot) < 5.7$  is  $-1.37 \pm 0.11$ . For star clusters with  $\log(M/M_\odot) < 4.5$ , where the mass function of massive star clusters starts to flatten out, the index  $\alpha$ , derived using star clusters younger than 10 Myr, is  $\alpha = -2.23 \pm 0.34$ . This index  $\alpha$  of young star clusters is in agreement with the cluster mass function index  $\alpha = -2.1 \pm 0.3$  reported by Bik et al. (2003) but it is slightly lower than  $\alpha = -1.70 \pm 0.08$  given by Gieles et al. (2006) for M51 star clusters. It is, however, in agreement with the cluster initial mass function (CIMF) index  $\alpha \approx -2.0$  of star clusters in late type galaxies (Zhang & Fall 1999; de Grijs et al. 2003;

Gieles et al. 2006).

The overall shape of the mass function of Class 1 and Class 2 star clusters is similar to each other. However, the mass function of Class 2 clusters appears to be slightly steeper than that of Class 1 clusters. That is, the power law index  $\alpha$  is  $-2.13 \pm 0.35$  for young ( $< 10$  Myr) and  $-1.62 \pm 0.37$  for old ( $> 100$  Myr) Class 2 clusters, while  $\alpha = -1.03 \pm 0.21$  for young and  $-1.27 \pm 0.14$  for old Class 1 clusters. Although the indices for old clusters may be in agreement with each other considering a relatively large error associated with Class 2 clusters, the difference in the mass function indices for young Class 1 and Class 2 clusters is rather significant. As explained in Hwang & Lee (2008) and in Section 3, one big difference between Class 1 and Class 2 clusters is their morphologies: Class 1 clusters are in circular shape, while Class 2 clusters have elongated or irregular structures. This suggests that many low mass clusters are usually formed or embedded in elongated and irregular structures.

To test the effect of incompleteness on the star cluster mass function, we have investigated how different limiting magnitudes in  $U$  and  $V$  band affect the overall shape and the slope of the mass function of star clusters. We constructed the cluster mass function using star clusters selected with varying limiting magnitude conditions in  $U$  and  $V$  bands ranging from 23 to 21.5 mag, respectively, and derived a power law index  $\alpha$  of the mass function over the same mass range as shown in Figure 7. The resulting index  $\alpha$  for young clusters ( $\log t < 7$ ) turns out to be the same under the varying limiting magnitudes from  $U < 23$  to  $U < 21.5$  mag and from  $V < 23$  to  $V < 22$  mag, respectively. Even when the constraint is set to  $V < 21.5$  mag, the mass function index is  $\alpha = -1.88 \pm 0.57$ , which is still in agreement with  $\alpha = -2.23 \pm 0.34$  for young clusters shown in Figure 7(a). For old clusters ( $\log t > 8$ ), it is also found that the mass function index is  $\alpha \approx -1.30 \pm 0.20$  for all magnitude constraints in  $U$  and  $V$  bands. This indicates that the power law indices of the young and old cluster mass functions derived in this study are affected little by the incompleteness problem. This is because the power law fits were done using the mass limits set sufficiently high enough to avoid severe incompleteness problem.

### 5.3. Evolution of the Star Cluster Mass Function

The variation of the slope of mass function depending on star cluster age shown in Figure 7 suggests that the index of cluster mass function may be a function of time. The cluster mass function for given time is determined by the initial cluster mass function, the cluster disruption, and the fading below the detection limit, as well as the variable cluster formation rate. We investigated the mass function of star clusters that formed in different epochs and derived its power law index for each epoch using the combined set of Class 1 and 2 star clusters, and the result is shown in Figure 8. Age ranges were chosen to separate star clusters roughly according to different features in the age distribution, as shown in Figure 5.

Figures 8(a) through 8(e) show that the upper part in the mass function of star clusters in each epoch can be represented approximately by a single power law and that the slopes of mass function change depending on the epochs. The derived power law indices of mass function are  $\alpha = -2.23 \pm 0.34$  for  $\log t < 7.0$  (panel

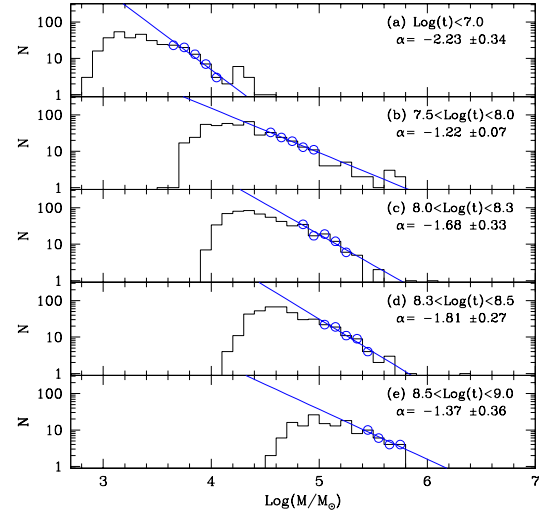


FIG. 8.— Mass functions of the star clusters in M51 for different age ranges (including both Class 1 and Class 2): (a)  $\log t < 7.0$ , (b)  $7.5 < \log t < 8.0$ , (c)  $8.0 < \log t < 8.3$ , (d)  $8.3 < \log t < 8.5$ , and (e)  $8.5 < \log t < 9.0$ . In each panel, the power law index of mass function is derived by fitting data points marked by circles and the solid line represents the best fit. Solid lines represent the power law fits to the data (marked by circles) for given mass ranges, and the resulting power law index for each age range is given in each panel (including both Class 1 and Class 2).

a),  $\alpha = -1.22 \pm 0.07$  for  $7.5 < \log t < 8.0$  (panel b),  $\alpha = -1.68 \pm 0.33$  for  $8.0 < \log t < 8.3$  (panel c),  $\alpha = -1.81 \pm 0.27$  for  $8.3 < \log t < 8.5$  (panel d), and  $\alpha = -1.37 \pm 0.36$  for  $8.5 < \log t < 9.0$  (panel e). These results are consistent with those in Figure 7 in the sense that the mass function of star clusters younger than  $\log t = 7$  is steeper than that of older star clusters. However, one interesting point in Figure 8 is that the mass function of star clusters with  $7.5 < \log t < 8.5$  gets steeper as ages increase. Especially, for star clusters with  $8.3 < \log t < 8.5$  shown in Figure 8(d), the power law index  $\alpha = -1.81 \pm 0.27$  is roughly in agreement with that of young star clusters shown in Figure 8(a). It is also noted that the relatively shallow mass function of star clusters with  $\log t > 8.5$  ( $\alpha = -1.37 \pm 0.36$ ) is consistent with that of star clusters with  $\log t > 8.0$  ( $\alpha = -1.37 \pm 0.11$ ) shown in Figure 7.

Since the cluster mass function index changes systematically depending on the epoch of star cluster formation, we investigated the power law index of cluster mass function using star clusters with  $\log t = 7.5 - 8.6$  when the condition of star cluster formation is expected to change drastically. The width of the logarithmic age bin was set to  $\delta \log t = 0.20$  and  $0.15$  to keep the number of star clusters more than 100 in each logarithmic bin, whenever it is possible. The maximum number of clusters in a single bin is about 420 and the minimum is about 70. We verified that the resulting cluster mass function in each logarithmic age bin can be always represented by a power law function and derived the index of mass function.

Figure 9 displays the power law indices of mass functions derived from logarithmic age bins with  $\delta \log t = 0.20$  (squares) and  $0.15$  (triangles). If the power law index was derived using more than 100 star clusters in each age bin, then the corresponding symbol is plotted in solid line. Otherwise, the symbol is marked in dotted

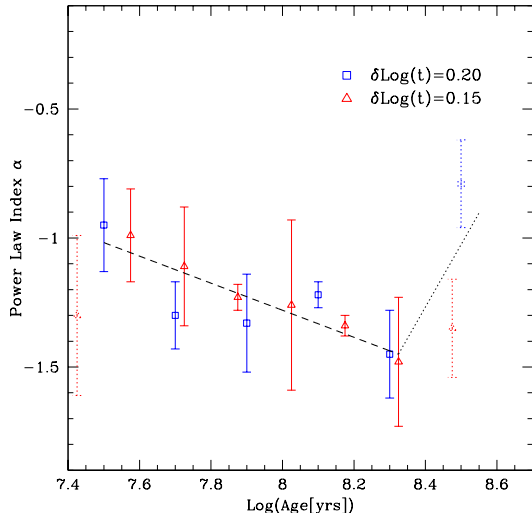


FIG. 9.— Mass function power law index vs. age of the star clusters in M51 (including both Class 1 and Class 2). The mass function index was derived for two logarithmic age bins,  $\delta \log t = 0.15$  (triangles) and 0.20 (squares). Note that the mass function index shows a minimum value (the steepest) at  $\log t \approx 8.3$ . Approximate linear fits are drawn for  $(t) < 8.3$  (dashed line) and  $\log t > 8.3$  (dotted line).

line. Figure 9 shows that, as we move to the higher age domain starting from  $\log t \approx 7.5$ , the star cluster mass function gets steeper, reaching  $\alpha \approx -1.50$  at  $\log t \approx 8.3$ , as shown in the dashed line derived from a simple linear fit. Then, the trend is reversed and the mass function gets shallower again for  $\log t > 8.4$ . However, the number of star clusters used to derive the index at  $\log t \approx 8.5$  is smaller than 100 (about 70) and the scatter between indices marked by a square and a triangle in dotted lines is large. This suggests significant uncertainties due to the limited number of massive star clusters available in this age domain (see Figure 4).

Interestingly, the epoch of  $\log t \approx 8.3$ , when the cluster mass function index seems to attain its minimum value, almost coincides with the age distribution peak at  $\log t \approx 8.4$  as shown in Figure 5. This period is also coincident with the epoch of dynamical encounter of the two galaxies NGC 5194 and NGC 5195 expected by theoretical models (Toomre & Toomre 1972; Salo & Laurikainen 2000). Therefore, the minimum value of cluster mass function index around this period may have some implications related with the increased number of star clusters and the dynamical interactions of the two galaxies in the M51 system. However, if the cluster mass function was affected and the number of star clusters increased during the course of dynamical interactions of galaxies, then there should be some impacts on the star cluster formation rate, which we focus on in the following section.

#### 5.4. Star Cluster Formation Rate

The cluster formation rate is a good indicator of the star formation activity. However, one of the difficulties of investigating the star cluster formation history is that more star clusters disappear due to the fading and/or the disruption as well as the observation incompleteness as we analyze older star cluster populations. Another difficulty is that, as shown in Figures 8 and 9, the star

cluster mass function does not appear to be constant but to evolve depending on the formation epochs. This suggests that the number of faint star clusters that we failed to detect may be different in different age bins, which makes the estimation of the number of the lost star clusters even more complicated.

Although the slope of the star cluster mass function depends on the epoch, the mass function itself can always be represented by a power law function, as shown in Figure 8. Therefore, based on the assumption that every star cluster mass function has a power law form, we constructed a ‘simple model’ mass function of star clusters by extrapolating the power law fitted mass function over  $\log t \approx 7.5 - 8.6$  period. This extrapolation method allows to compensate the number of star clusters lost due to the detection limit and the incompleteness problem of the observed data. However, this method does *not* correct for star cluster disruption. For the model mass function, we set the lower mass limit to  $10^3 M_\odot$  and the upper mass limit to  $10^{6.5} M_\odot$ , since there is no star cluster with more massive than  $10^{6.5} M_\odot$  in our data, as shown in Figure 7.

Using these simple model and observed mass functions, we calculated the number of star clusters per each Myr, i.e., the star cluster formation rate, in each logarithmic age bin over  $7.5 < \log t < 8.6$ . For this investigation, two mass limited samples of star clusters were chosen by selecting star clusters with  $\log(M/M_\odot) > 5.0$  and  $4.6 < \log(M/M_\odot) < 5.0$ . These criteria were defined to select star clusters located above the detection limit of  $U = 22$  mag (see Figure 4) and the completeness of about 80% (see Figure 3) at  $\log t \lesssim 8.8$  for  $\log(M/M_\odot) > 5.0$  and at  $\log t \lesssim 8.5$  for  $4.6 < \log(M/M_\odot) < 5.0$ . The definition of mass limited cluster samples also helps to avoid any possible artificial contribution from the low mass part of the model mass function, and enables to test whether any discrepancy in cluster formation rate exists between different mass ranges.

Figure 10 displays the age distribution and cluster formation rate derived from star clusters with  $\log(M/M_\odot) > 5.0$  (panels a and c) and  $4.6 < \log(M/M_\odot) < 5.0$  (panels b and d). Solid lines are from the observed data, while dashed lines are from the model mass function. The observed data of star clusters with  $\log(M/M_\odot) > 5.0$  reveal a peak in the age distribution and an abrupt increase of the cluster formation rate at  $\log t \approx 8.4$ , as shown in Figures 10(a) and (c). Then, the data exhibit a gradual decrease in the age distribution and a rough plateau in the cluster formation rate in  $7.8 < \log t < 8.4$ . Very similar features are seen in the age distribution and cluster formation rate of star clusters with  $4.6 < \log(M/M_\odot) < 5.0$  in Figures 10(b) and (d). The peak at  $\log t \approx 8.4$  shown in the age distribution and the cluster formation rate is consistent with the peak in the age distribution found around  $\log t = 8.4$  as shown in Figure 5.

The data from model mass function also display a peak at  $\log t \approx 8.4$  in the age distribution shown by dashed lines in Figures 10(a) and (b). However, for star clusters with  $\log(M/M_\odot) > 5.0$ , one slightly different feature is a bump-like peak at  $\log t \approx 7.8$  in the age distribution in Figure 10(a). Although this feature does not appear significant, it seems to translate into another peak of the cluster formation rate at  $\log t \approx 7.8$  apart from the one

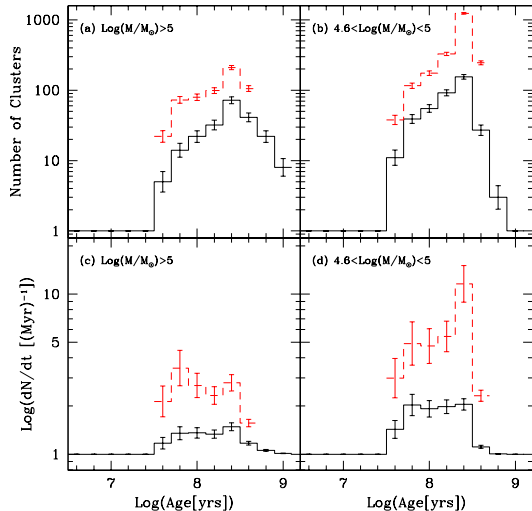


FIG. 10.— Age distributions (a and b) and cluster formation rates as a function of age (c and d) for two mass ranges:  $\log(M/M_{\odot}) > 5.0$  (a and c) and  $4.6 < \log(M/M_{\odot}) < 5.0$  (b and d). Solid line histograms represent the observed data and dashed line histograms represent the simple model data. Note that there is seen a peak at  $\log t \approx 8.4$  in the age distributions for both mass ranges and in the cluster formation rate derived from the model data for the lower mass range.

at  $\log t \approx 8.4$  in Figure 10(c). For star clusters with  $4.6 < \log(M/M_{\odot}) < 5.0$ , no such a bump-like feature is seen in the age distribution and no cluster formation rate peak exists at  $\log t \approx 7.8$ , as shown in Figures 10(b) and (d). The model mass function data reproduce main features exhibited by the observed data, including a peak at  $\log t \approx 8.4$  and a gradual decrease in the age distribution, and a plateau in the cluster formation rate in  $7.8 < \log t < 8.4$ .

Figure 10 shows that star cluster formation rate was raised at  $\log t \approx 8.4$  and was maintained in that heightened state for somewhat extended period until  $\log t \approx 7.8$ . This is true for star clusters with both  $\log(M/M_{\odot}) > 5.0$  and  $4.6 < \log(M/M_{\odot}) < 5.0$ . However, it is also probable that massive star clusters with  $\log(M/M_{\odot}) > 5.0$  have experienced more than one burst of cluster formation: one at  $\log t \approx 8.4$  and another at  $\log t \approx 7.8$ . On the other hand, according to the model mass function, star clusters with  $4.6 < \log(M/M_{\odot}) < 5.0$  exhibit one strong peak of the cluster formation rate at  $\log t \approx 8.4$ .

## 6. DISCUSSION

### 6.1. Star Cluster Formation and Dynamical Interactions of Galaxies

The age distribution shown in Figure 5 displays two peaks at  $\log t \approx 8.0$  and  $\approx 8.4$ . Interestingly, the epochs of these two peaks coincide with the dynamical interaction epochs predicted by the multiple encounter model of M51 system (Salo & Laurikainen 2000). However, if the size of logarithmic age bin is enlarged from the current value  $\delta \log t = 0.15$  to  $\delta \log t = 0.2$ , then those two age peaks merge into one broad component ranging over  $\log t = 8.0 - 8.4$ . In this case, it is not straightforward to confirm the existence of independent peaks in the star cluster age distribution and the possible correlation between those peaks and the individual dynamical inter-

actions, even though it is still clear that a large population of star clusters were formed during this period of  $\log t = 8.0 \sim 8.4$ . The uncertainty is mostly due to the typical error in age estimation based on the broad band SED fit technique, about 20% (Anders et al. 2004; de Grijs et al. 2003).

Figure 10 shows that the star cluster formation rate increased over the same period of  $\log t = 8.0 \sim 8.4$ . Moreover, more than one event of significant cluster formation rate increase are apparent at  $\log t \approx 8.4$  and  $\log t \approx 7.8$ , depending on the mass of star clusters. However, the cluster formation peak at  $\log t \approx 7.8$  is slightly apparent only from the model data for massive star clusters with  $\log(M/M_{\odot}) > 5$ . It may be possible that the peak at  $\log t \approx 7.8$  was made by some stochastic effect and that it may not be a real feature because the peak is not so strong and involves a relatively large error. However, this recent peak in the cluster formation rate is noted to be nearly coeval with the peak in the age distribution at  $\log t \approx 8.0$ , as shown in Figure 5.

Except for the SED fit error, the star cluster disruption and the evolution of luminosity and mass function can affect the star cluster age distribution and cluster formation rate. Although many uncertainties are related with these, it is relatively well known from the theoretical and observational studies (Fall 2006; Larsen 2009) that the luminosity function and mass function of young star clusters follow, in most cases, power law functions with a single parameter  $\alpha$  that defines its slope. Hwang & Lee (2008) showed that the luminosity function of M51 star clusters is fitted by a single power law with  $\alpha = -2.59 \pm 0.03$ , which is in good agreement with the results in other studies of M51 star clusters,  $\alpha = -2.5 \pm 0.1$  by Gieles et al. (2006) and  $\alpha = -2.53 \pm 0.06$  by Haas et al. (2008).

Figure 8 shows that the mass function of star clusters with different formation epochs can be also described with a single power law, although the mass function index seems to change depending on the epochs. Even when we select star clusters from a single logarithmic age bin to construct a mass function, the resulting mass function is found to follow a single power law over a period of  $\log t \approx 7.5 \sim 8.6$ . However, Figure 9 shows that the mass function appears to evolve depending on the cluster formation epoch. That is, the mass function gets steeper as star clusters get older until  $\log t \approx 8.3$  when the index reaches the minimum value  $\alpha \approx -1.50$ , making the steepest mass function. Then, the mass function appears to overturn to become a shallower function as star clusters get older than  $\log t \approx 8.3$ .

The change in the mass function slope may be explained as a result of the evolution of star clusters. Especially, the cluster mass function can be shallower due to the selective disruption of low mass star clusters. This is one of the reasons why the mass function of star clusters older than 100 Myr ( $\alpha = -1.37 \pm 0.11$ ) is flatter than that of star clusters younger than 10 Myr ( $\alpha = -2.23 \pm 0.34$ ) as noted in Section 5.2. However, Figure 9 shows that the mass function gets steeper reaching the power law index  $\alpha \approx -1.50$  at  $\log t \approx 8.3$ . If we assume that the star cluster disruption and evolutionary fading should apply to all star clusters consistently regardless of their formation epochs, the change in the mass function slope suggests that the number of star clusters increased sig-

nificantly around the epoch of  $\log t = 8.3$ .

What our results show is that many star clusters are formed around  $\log t = 8.4$  (250 Myr ago) and this period is roughly in agreement with the first encounter period of NGC 5194 and NGC 5195 predicted by theoretical models (Toomre & Toomre 1972; Salo & Laurikainen 2000). This may suggest that the dynamical interaction between two galaxies in the M51 system induced star cluster formation, implying a strong correlation between the active star cluster formation and the dynamical interactions experienced by the host galaxies. This is also in agreement with the result of Lee et al. (2005) that the number of star clusters with 100 – 400 Myr is significantly larger in M51 than in other late type galaxy M101, suggesting a correlation between the increased number of star clusters and the dynamical interaction(s) at the similar epoch.

There is a hint, although weak, for another increase of cluster formation rates around  $\log t = 7.8$ , e.g., as shown in Figure 10(c). In a study on the cluster formation in M51, Bastian et al. (2005) reported the existence of relatively recent star cluster bursts in M51: one at  $\approx 6$  Myr ( $\log t \approx 6.8$ ) and another at  $\approx 60$  Myr ( $\log t \approx 7.8$ ). The latter burst coincides with the probable increase of star cluster formation at  $\log t \approx 7.8$ . The former star cluster burst is reproduced as a peak at  $\log t \approx 6.7$  in the star cluster age distribution shown in Figure 5. No report about the increase of star cluster formation in  $\log t > 8.0$  was given in Bastian et al. (2005). However, it is noted that a weak hint is apparent in their Figure 12 that implies a slight increase of cluster formation rate at  $\log t \approx 8.5$  for star clusters with  $\log(M/M_\odot) > 4.7$ .

### 6.2. Star Cluster Disruption and Age Distribution

Among many studies in the literature, Lamers (2008) described very concisely two major models that are used for studies of star cluster age distribution, i.e., the ‘Baltimore model’ (Fall et al. 2005) and the ‘Utrecht model’ (Boutloukos & Lamers 2003). The Baltimore model is characterized by the mass independent disruption of about 90% star clusters in each age dex up to approximately 1 Gyr. On the other hand, the Utrecht model includes the evolutionary fading and the mass dependent dynamical cluster dissolution by tidal effects as well as the mass independent dissolution of star clusters in their very early stages, which they termed as ‘infant mortality’. These two models predict different outcomes in the distribution of maximum cluster mass in each age dex (Gieles & Bastian 2008) and in the cluster age distribution in a  $\log(dN/dt)$  versus  $\log(t)$  plane (Lamers 2008). We use our age and mass data of M51 star clusters to test these two models.

One way to derive the cluster disruption rate is to use the relation between mass and age of star clusters and a ‘size of sample’ effect that more massive star clusters are found in older logarithmic age bins, as shown in Figure 4. This effect comes from the assumption that when star clusters are randomly selected from a physically determined mass function, the larger samples are likely to have the more massive star clusters. Hunter et al. (2003) described how to derive the CIMF index  $\alpha$ , independent of cluster disruption and evolutionary fading rates from the slope defined using the maximum mass and the age of star clusters, assuming a constant cluster formation.

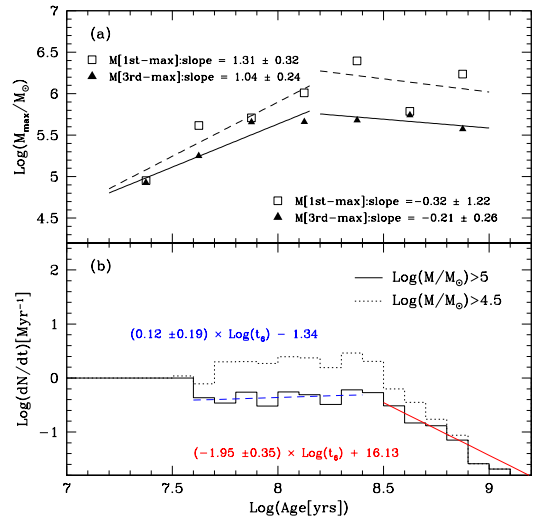


FIG. 11.— (a) The 1st (squares) and 3rd (triangles) maximum mass vs. age of the star clusters in M51 (including both Class 1 and Class 2). Note that there is a break at  $\log t \approx 8.2$ . Dashed lines and solid lines represent linear fits to the data for the 1st and 3rd maximum masses, respectively. (b) Cluster formation rate vs. age of the star clusters in M51 (including both Class 1 and Class 2) for two mass ranges:  $\log(M/M_\odot) > 5$  (solid line histogram) and  $\log(M/M_\odot) > 4.5$  (dotted line histogram). Linear fits to flat and steep parts are plotted in dashed and solid lines, respectively.

Gieles & Bastian (2008) expanded this by showing that this slope is also an indicator for the mass independent disruption rate of star clusters when we have information about the CIMF. The Baltimore model expects about 90% star clusters in each logarithmic age bin to disrupt regardless of their mass, which would result in a flat distribution as shown in Gieles & Bastian (2008).

Figure 4 shows that, although it is hard to define due to large scatters, the upper limit of mass and age distribution of M51 star clusters appears to be composed of roughly two linear components:  $7.0 < \log t < 8.2$  and  $\log t > 8.2$ . Figure 11(a) displays this distribution of the maximum mass (open square) and the 3rd maximum mass (filled triangle) of M51 star clusters in each logarithmic age bin with a step of  $\delta \log t = 0.25$ . A linear square fit to  $\log t < 8.2$  returns a slope of  $1.31 \pm 0.32$  for the maximum mass and  $1.04 \pm 0.24$  for the 3rd maximum mass, while another fit to  $\log t > 8.2$  returns  $-0.32 \pm 1.22$  for the maximum mass and  $-0.21 \pm 0.26$  for the 3rd maximum mass. If we fit this distribution with a single line over the range of  $7.0 < \log t < 9.5$ , the slope turns out to be  $0.72 \pm 0.23$ . This value is steeper than 0.4 reported by Lee et al. (2005),  $0.26 \pm 0.09$  by Gieles et al. (2006), and 0.23 by Gieles & Bastian (2008) for M51 star clusters.

This shows that the maximum mass distribution for young star clusters with  $\log t < 8.2$  is steep, while that for old star clusters with  $\log t > 8.2$  is more or less flat. The slope of the steep part is even slightly steeper than 0.74 for LMC and 0.69 for SMC reported by Hunter et al. (2003), although the slope of about 0.72 derived over  $7.0 < \log t < 9.5$  is in good agreement with these. However, the steep slope derived from star clusters with  $\log t < 8.2$  is consistent with those derived from LMC (0.96) and SMC (0.93) clusters with  $\log(t) < 8.0$  by

Gieles & Bastian (2008). On the other hand, for the Antennae galaxy, Gieles & Bastian (2008) show that the slope is 0.01 for clusters with  $\text{Log}(t) < 8.0$ , which is consistent with the Baltimore model. These results suggest that the Baltimore model, at least, does not apply to M51 star clusters, considering that the flat distribution of maximum mass in  $\log t > 8.2$  may be due to the physical upper limit of M51 star cluster mass (Gieles et al. 2006).

Figure 11(b) displays the age distribution of the mass limited star clusters in a  $\log dN/dt$  versus  $\log t$  plane. It clearly shows a bend at  $\log t \approx 8.4$  and the existence of a plateau over  $\log t \approx 7.6 - 8.4$ , which is a characteristic of the Utrecht model. On the contrary, the Baltimore model expects a consistently decreasing relation as shown by Fall et al. (2005) in their Figure 2. Even when we change the mass limit, the result is still consistent for  $\log(M/M_\odot) > 5.0$  (solid line) and for  $\log(M/M_\odot) > 4.5$  (dotted line). Applying a simple linear fit returns a slope of  $0.12 \pm 0.19$  for the plateau (dashed line) and  $-1.95 \pm 0.35$  for the steep part at  $\log t > 8.4$  (solid line). This slope  $-1.95 \pm 0.35$  of the steep part is in agreement with the value ( $\approx -1.7$ ) expected by the Utrecht model considering the error (Lamers 2008). If we apply the analysis of Boutloukos & Lamers (2003) relating this slope  $A$  to the CIMF slope  $\alpha$ , we can derive the dynamical disruption parameter  $\gamma$  from the equation  $A = (1 + \alpha)/\gamma$  (for  $\alpha < 0$ ). If we assume the CIMF with  $\alpha = -2.0$ , then the disruption parameter is  $\gamma = 0.53 \pm 0.10$ . This is in good agreement with the result  $0.57 \pm 0.10$  reported by Lamers et al. (2005) for M51. Therefore, the age distribution of M51 star clusters can be described better by the Utrecht model than by the Baltimore model and the cluster disruption parameter derived from our data is in agreement with the literature.

### 6.3. Correlation of Cluster Size with Age and Mass

The mass of a star cluster is expected to be proportional to the cluster size since a star cluster would form from a parent molecular cloud once it reaches a critical density. If we assume a constant density for a cluster, the cluster size would increase in proportion to  $M^{1/3}$ . However, it was found by Larsen (2004) based on the investigation of young star clusters in 18 nearby spiral galaxies that the correlation between the half light radius  $r_{\text{eff}}$  and the mass ( $M$ ) of star clusters returned a shallower slope than expected from a constant-density assumption. For M51 star clusters, Bastian et al. (2005) tried to find any correlation between the cluster size and mass but there was no apparent correlation in their data. More recently, Scheepmaker et al. (2007) also investigated the size distribution of star clusters using the *HST* ACS data and they also reported that they did not find evidence for any direct relation between mass and radius of the clusters. On the other hand, Lee et al. (2005) showed the correlation between the size and mass of star clusters with a best-fit slope of  $0.14 \pm 0.03$ , which is in agreement with the result of Larsen (2004) within  $1.5\sigma$ .

We have investigated the correlation of size with mass of star clusters. The sizes of star clusters were measured using ISHAPE package (Larsen 1999). Detailed information on the size measurement and size distribution of M51 star clusters was described in Hwang & Lee (2008).

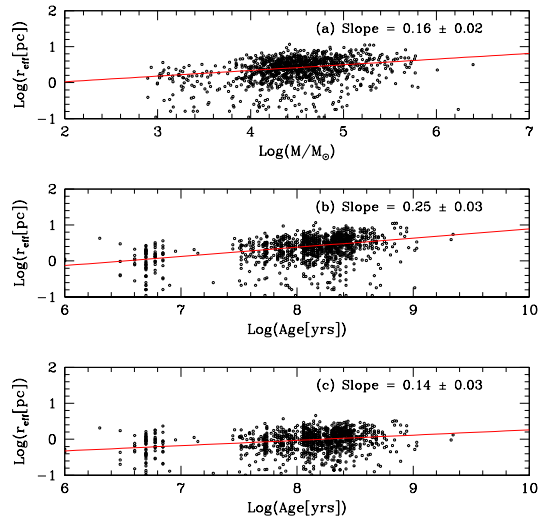


FIG. 12.— (a) Effective radius vs. mass, (b) effective radius vs. age, and (c) effective radius vs. mass corrected for the derived size-mass relation of the star clusters in M51 (including both Class 1 and Class 2). Solid lines represent the best power law fits (linear fits in the logarithmic scales).

Figure 12(a) shows the distribution of star cluster sizes and masses. The power law relation between these two parameters is clearly seen in this plot although with large scatters. We derived the best linear fit from this distribution with a slope of  $0.16 \pm 0.02$ , which is consistent with the result of Lee et al. (2005) at the  $\sim 1\sigma$  level. This correlation indicates that the cluster mass distribution in M51 is shallower than that expected from the constant density assumption.

Figure 12(b) shows the distribution of star cluster sizes and their ages. It is seen that there is a trend of cluster size increasing proportional to the cluster age and this is another result of the ‘size-of-sample’ effect discussed in Section 6.2. The best linear fit to the data, shown in a solid line, gives a slope of  $0.25 \pm 0.03$ . However, the observed size-age relationship may simply reflect the fact that the observed mass limit goes up with age, as shown in Figure 4. Therefore, in order to check whether there is an intrinsic trend between star cluster sizes and ages, we correct the derived star cluster mass-size relation and fit the data again, as shown in Figure 12(c). It results in a linear fit with a slope of  $0.14 \pm 0.03$ , which is steeper than  $0.06 \pm 0.02$  by Lee et al. (2005) and  $0.08 \pm 0.03$  by Scheepmaker et al. (2007). The relation is shallower than found before correcting the mass-size relation but it still shows that the size of star clusters increases with age. This result is in contradiction to that of Bastian et al. (2005) in which a slight trend of the decreasing size with increasing age was shown.

## 7. SUMMARY AND CONCLUSION

We present the age and mass distribution of about 2,000 star clusters in M51 based on the SED fit of *UBVI* photometric data. The star cluster age distribution displays two peaks at  $\log t \approx 8.0$  (100 Myr) and  $\log t \approx 8.4$  (250 Myr). These peaks roughly coincide with the epochs of dynamical encounters of NGC 5194 and NGC 5195 predicted by a multiple encounter model (Salo & Laurikainen 2000). The star cluster formation

rate derived from the age distribution suggests that the cluster formation rate increased significantly during the period of 100 ~ 250 Myr ago, when the dynamical interaction in M51 is expected by the theoretical models (Toomre & Toomre 1972; Salo & Laurikainen 2000).

The mass function of star clusters can be represented by a single power law, and the index  $\alpha$  appears to change depending on the formation epoch:  $\alpha \approx -2.23 \pm 0.34$  for  $t < 10$  Myr while  $\alpha \approx -1.37 \pm 0.11$  for  $t > 100$  Myr. Interestingly, the mass function index  $\alpha$  changes systematically depending on the formation epochs of star clusters and the star clusters with  $\log t \approx 8.3$  (200 Myr) displays the steepest mass function with  $\alpha \approx -1.50$  among star clusters older than 10 Myr. This also implies an increased star cluster formation at the corresponding epoch, possibly incurred by the dynamical interaction of host galaxies.

The correlation between the maximum mass of star clusters and the logarithmic age displays a steep slope of about 1.0 for  $\log t < 8.2$ , while it is more or less flat for  $\log t > 8.2$ . The age distribution of mass limited star clusters clearly displays the existence of a plateau over  $\log t \approx 7.6 - 8.4$  and a bend at  $\log t \approx 8.4$ . The steep slope of the maximum cluster mass and the existence of a bend in the mass limited age distribution indicates

that the disruption and evolution of M51 star clusters is described better with the Utrecht model than with the Baltimore model. The cluster disruption parameter  $\gamma$  derived following the analysis of Boutloukos & Lamers (2003) is  $\gamma = 0.53 \pm 0.10$  under the assumption of CIMF  $\alpha = -2.0$ , which is in good agreement with the result given by Lamers et al. (2005).

We found that the size of star clusters are positively correlated with the mass of star clusters with a best fit slope  $0.14 \pm 0.03$ . It shows that the size of star clusters increases with age even after the correction of the mass-size relation with a slope  $0.16 \pm 0.02$ .

The authors are grateful to Yanbin Yang for providing the SED fitting program and acknowledge the support of the BK21 program of the Korean Government. N.H. was supported in part by Grant-in-Aid for JSPS Fellow No. 20-08325. M.G.L was supported in part by a grant (R01-2007-000-20336-0) from the Basic Research Program of the Korea Science and Engineering Foundation. Finally, we thank an anonymous referee for critical and constructive comments that helped to improve the original manuscript.

#### REFERENCES

- Anders, P., Bissantz, N., Fritze-v. Alvensleben, U., & de Grijs, R. 2004, *MNRAS*, 347, 196
- Bastian, N., Gieles, M., Lamers, H. J. G. L. M., Scheepmaker, R. A., & de Grijs, R. 2005a, *A&A*, 431, 905
- Bertin, E., & Arnouts, S. 1996, *A&AS*, 117, 393
- Bik, A., Lamers, H. J. G. L. M., Bastian, N., Panagia, N., & Romaniello, M. 2003, *A&A*, 397, 473
- Boutloukos, S. G., & Lamers, H. J. G. L. M. 2003, *MNRAS*, 338, 717
- Bruzual, & Charlot, 2003, *MNRAS*, 344, 1000
- de Grijs, R., Fritze-v. Alvensleben, U., Anders, P., Gallagher, J. S., Bastian, N., Taylor, V. A., & Windhorst, R. A. 2003, *MNRAS*, 342, 259
- de Vaucouleurs, G. et al. 1991, *Third Reference Catalog of Bright Galaxies* (Berlin:Springer)
- Diaz, A. I., Terlevich, E., Vilchez, J. M., Pagel, B. E. J., & Edmunds, M. G. 1991, *MNRAS*, 253, 245
- Dolphin, A. 2000, *PASP*, 112, 1397
- Durrell, P. R., Mihos, J. C., Feldmeier, J. J., Jacoby, G. H., & Ciardullo, R. 2002, *ApJ*, 582, 170
- Fall, S. M., Chandar, R., & Whitmore, B. C. 2005, *ApJ*, 631, L133
- Fall, S. M. 2006, *ApJ*, 652, 1129
- Feldmeier, J. J., Ciardullo, R., & Jacoby, G. H. 1997, *ApJ*, 479, 231
- Gieles, M., Bastian, N., Lamers, H. J. G. L. M., & Mout, J. N. 2005, *A&A*, 441, 949
- Gieles, M., Larsen, S. S., Bastian, N., & Stein, I. T. 2006, *A&A*, 450, 129
- Gieles, M., & Bastian, N. 2008, *A&A*, 482, 165
- Hass, M. R., Gieles, M., Scheepmaker, R. A., Larsen, S. S., & Lamers, H. J. G. L. M. 2008, *A&A*, 487, 937
- Hill, J. K. et al. 1997, *ApJ*, 477, 673
- Hunter, D. A., Elmegreen, B. G., Dupuy, T. J., & Mortonson, M. 2003, *AJ*, 126, 1836
- Hwang, N., & Lee, M. G. 2006, *ApJ*, 638, L79
- Hwang, N., & Lee, M. G. 2007, *IAU Symposium*, 241, *Stellar Populations as Building Blocks of Galaxies*, Eds. A. Vazdekis, & R. Peletier (Cambridge: Cambridge University Press), 451
- Hwang, N., & Lee, M. G. 2008, *AJ*, 135, 1567
- Lamers, H. J. G. L. M. et al. 2002, *ApJ*, 566, 818
- Lamers, H. J. G. L. M., Gieles, M., & Zwart, S. F. P. 2005, *A&A*, 429, 173
- Lamers, H. J. G. L. M. 2008, arXiv:0804.2148
- Larsen, S. S. 1999, *A&AS*, 139, 393
- Larsen, S. S. 2004, *A&A*, 416, 537
- Larsen, S. S. 2009, *A&A*, 494, 539
- Lee, M. G., Chandar, R., & Whitmore, B. W. 2005, *AJ*, 130, 2128
- Mutchler, M. et al. 2005, *BAAS*, 37, 2
- Salo, H., & Laurikainen, E. 2000a, *MNRAS*, 319, 377
- Salpeter, E. E. 1955, *ApJ*, 121, 161
- Scheepmaker, R. A., Haas, M. R., Gieles, M., Bastian, N., Larsen, S. S., & Lamers, H. J. G. L. M. 2007, *A&A*, 469, 925
- Scheepmaker, R. A., Lamers, H. J. G. L. M., Anders, P., & Larsen, S. S. 2009, *A&A*, 494, 81
- Schlegel, D. J., Finkbeiner, D. P., & Davis, M. 1998, *ApJ*, 500, 525
- Schuster, K. F., Kramer, C., Hitschfeld, M., Garcia-Burillo, S., & Mookerjee, B. 2007, *A&A*, 461, 143
- Scoville, N. Z., Polletta, M., Ewald, S., Stolovy, S. R., Thompson, R., & Rieke, M. 2001, *AJ*, 122, 3017
- Sirianni, M., et al. 2005, *PASP*, 117, 1049
- Toomre, R. P. J., & Toomre, J. 1972, *ApJ*, 178, 623
- Zhang, Q., & Fall, S. M. 1999, *ApJ*, 527, L81